Tunneling of obliquely incident waves through $\mathcal{PT}$-symmetric epsilon-near-zero bilayers

Silvio Savoia, Giuseppe Castaldi, and Vincenzo Galdi*
Waves Group, Department of Engineering, University of Sannio, I-82100 Benevento, Italy

Andrea Alù
Department of Electrical and Computer Engineering, The University of Texas at Austin, Austin, Texas 78712, USA

Nader Engheta
Department of Electrical and Systems Engineering, University of Pennsylvania, Philadelphia, Pennsylvania 19104, USA

(Received 11 December 2013; revised manuscript received 20 January 2014; published 6 February 2014)

We show that obliquely incident, transversely magnetic-polarized plane waves can be totally transmitted (with zero reflection) through *epsilon-near-zero* (ENZ) bilayers characterized by balanced loss and gain with *parity-time* ($\mathcal{PT}$) symmetry. This tunneling phenomenon is mediated by the excitation of a surface wave localized at the interface separating the loss and gain regions. We determine the parameter configurations for which the phenomenon may occur and, in particular, the relationship between the incidence direction and the electrical thickness. We show that, below a critical threshold of gain and loss, there always exists a tunneling angle which, for moderately thick (wavelength-sized) structures, approaches a critical value dictated by the surface-wave phase-matching condition. We also investigate the *unidirectional* character of the tunneling phenomenon, as well as the possible onset of *spontaneous symmetry breaking*, typical of $\mathcal{PT}$-symmetric systems. Our results constitute an interesting example of a $\mathcal{PT}$-symmetry-induced tunneling phenomenon, and may open up intriguing venues in the applications of ENZ materials featuring loss and gain.

DOI: 10.1103/PhysRevB.89.085105 PACS number(s): 42.25.Bs, 78.67.Pt, 78.20.Ci, 11.30.Er

I. INTRODUCTION

In a series of seminal works by Bender and co-workers [1–3], it was shown that, in spite of the standard axioms in quantum mechanics, a *non-Hermitian* Hamiltonian characterized by the so-called *parity-time* ($\mathcal{PT}$) symmetry can still exhibit an *entirely real* energy eigenspectrum. Similar concepts had also been previously explored within the framework of atomic physics [4].

In essence, a $\mathcal{PT}$-symmetric Hamiltonian commutes with the combined *parity* (i.e., space reflection $\mathbf{r} \to -\mathbf{r}$) and *time-reversal* ($t \to -t$, or complex conjugation * in the time-harmonic regime) operator [3]. This implies that the quantum potential satisfies the symmetry condition $V(\mathbf{r}) = V^*(-\mathbf{r})$. However, the latter is only a *necessary* condition for the so-called "exact" phase characterized by a *real* eigenspectrum. Beyond some non-Hermiticity threshold, an abrupt phase transition may occur to the so-called "broken" phase characterized by a *complex* eigenspectrum [3]. Such phenomenon, typically referred to as *spontaneous symmetry breaking*, may occur since the Hamiltonian and the (antilinear) $\mathcal{PT}$ operators do not necessarily share the same eigenstates [3].

More recently, the $\mathcal{PT}$-symmetry concept has elicited a great deal of interest within the fields of optics, photonics, and plasmonics. Theoretically founded on the formal analogies between Helmholtz and Schrödinger equations, such interest is motivated by the relatively simpler (by comparison with quantum physics) conception and realization of $\mathcal{PT}$-symmetric electromagnetic structures by means of spatially modulated distributions of loss and gain, either across or along the wave-propagation direction. Within this framework, the arguably simplest scenario consists of coupled optical waveguides, either in passive, lossy configurations [5] (which, after appropriate transformations, are pseudo-$\mathcal{PT}$-symmetric) or in the actual presence of loss and gain [6]. Starting from these simpler configurations, a number of different $\mathcal{PT}$-symmetry-inspired phenomena and effects have been studied in optical, plasmonic, and metamaterial structures, from both theoretical/numerical [7–24] and experimental [25–27] sides. Aside from the very intriguing application-oriented perspectives in the development of novel devices and components (e.g., switches, lasers, absorbers), optical and photonic analogies may also serve as more feasible experimental test beds for controversial $\mathcal{PT}$-symmetry-induced quantum-field effects [28]. Also worthy of mention is the research field of $\mathcal{PT}$-symmetric electronics, based on circuit implementations where gain can naturally be introduced via amplifiers [29,30].

A particularly simple and yet very insightful $\mathcal{PT}$-symmetric optical configuration is obtained by pairing two material slabs characterized by permittivities (and/or permeabilities) with the same real part and opposite imaginary parts, i.e., loss at one side and gain at the other side. In the topical literature, such $\mathcal{PT}$-symmetric bilayers have been studied extensively under normally incident plane-wave illumination, showing intriguing anomalous effects such as spectral singularities [7], coherent perfect absorption [13], and anisotropic transmission resonances [17]. Against this background, in this paper, we deal instead with *oblique* plane-wave illumination. We show that, for suitable field polarization and constitutive parameters, a propagating plane-wave obliquely impinging from vacuum may effectively tunnel (with zero reflection) through the $\mathcal{PT}$-symmetric bilayer. This phenomenon is mediated by the excitation of a localized surface wave at the interface separating the gain and loss

*vgaldi@unisannio.it

regions, and generally exhibits a *unidirectional* character, i.e., zero reflection is achieved only when exciting the structure from one side and not from the other.

In particular, we focus on the *epsilon-near-zero* (ENZ) regime, i.e., vanishingly small real part of the permittivities, for which the above phenomena may be observed even in the presence of reasonably low levels of loss and gain, and moderately thick structures. Recently, ENZ materials have gained a growing attention [31], and their application has been suggested in a variety of scenarios including, among others, supercoupling [32], tailoring the radiation phase pattern of sources [33], dielectric sensing [34], enhancing the photon density of state for embedded emitters [35,36], boosting nonlinear effects [37–39], subwavelength image manipulation [40], nonlocal transformation optics [41], and field enhancement [42]. Moreover, for these materials, the effects of loss and gain have been studied in connection with loss compensation [43–45], perfect absorption and giant magnification [46], loss-enhanced transmission and collimation [47], coherent-perfect absorption [48], loss-induced omnidirectional bending [49], and gain-assisted harmonic generation [50]. Our study here provides a new perspective in the effect of balanced loss and gain in ENZ materials.

The rest of the paper is organized as follows. After an outline of the problem (geometry, assumptions, and observables) in Sec. II, we present the main analytical derivations and numerical results (Sec. III), with details relegated in three appendices. In connection with the tunneling condition, we identify three regimes of operation (depending on the loss/gain level), and the possible presence of a critical tunneling angle dictated by the dispersion law of the surface wave excited at the interface separating the loss and gain regions. We also study the *unidirectional* character of the phenomenon, as well as the onset of spontaneous symmetry breaking (Sec. IV) and, finally, provide some conclusions and perspectives (Sec. V).

II. PROBLEM STATEMENT

A. Geometry and assumptions

As illustrated in Fig. 1, the geometry of interest features an isotropic, nonmagnetic (i.e., relative permeability $\mu = 1$), piecewise homogeneous $\mathcal{PT}$-symmetric bilayer immersed in vacuum. The bilayer is composed of two slabs of identical thickness d (and infinite extent along the x, y directions) paired along the z direction, characterized by complex-conjugate relative permittivities ε_1 and ε_1^*, respectively, so as to fulfill the necessary condition for $\mathcal{PT}$ symmetry $\varepsilon(z) = \varepsilon^*(-z)$. Under time-harmonic $[\exp(-i\omega t)]$ time convention, we assume

$$\varepsilon_1 = \varepsilon' - i\varepsilon'', \quad \varepsilon' > 0, \quad \varepsilon'' > 0, \tag{1}$$

so that the left and right halves ($-d < z < 0$ and $0 < z < d$, respectively) are characterized by gain and loss, respectively. Moreover, we focus on the ENZ limit

$$\varepsilon' \ll \varepsilon'' \ll 1. \tag{2}$$

We are interested in studying the electromagnetic response under transverse-magnetic (TM) plane-wave illumination obliquely incident from either sides (cf. Fig. 1). Accordingly, we consider a unit-amplitude, y-directed magnetic field ($H_l^{(i)}$ or $H_r^{(i)}$)

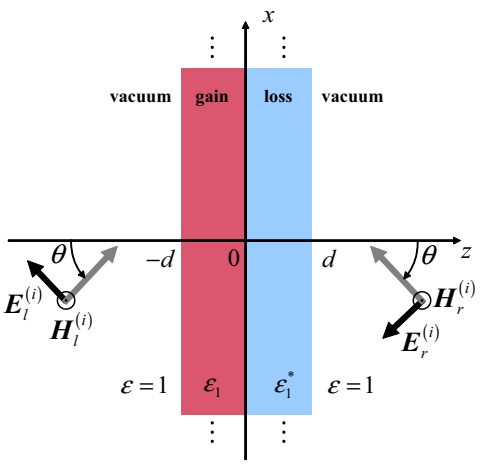

FIG. 1. (Color online) Problem geometry. A $\mathcal{PT}$-symmetric bilayer composed of two halves of identical thickness d, and relative permittivities $\varepsilon_1 = \varepsilon' - i\varepsilon''$ ($\varepsilon'' > 0$, i.e., gain) and $\varepsilon_1^* = \varepsilon' + i\varepsilon''$ (loss), immersed in vacuum, is illuminated by a TM-polarized plane wave obliquely impinging from the left or right side.

$$H_{l,r}^{(i)}(x,z) = \exp\left[i\left(k_{x0}x \pm k_{z0}z\right)\right], \tag{3}$$

where the subscripts l and r (and $+$ and $-$ signs) denote the incidence from the left and right, respectively. For propagating waves with incidence angle θ (cf. Fig. 1), the wave numbers k_{x0} and k_{z0} can be expressed as

$$k_{x0} = k_0 \sin\theta, \quad k_{z0} = k_0 \cos\theta, \tag{4}$$

in terms of the vacuum wave number $k_0 = \omega/c_0 = 2\pi/\lambda_0$ (with c_0 denoting the speed of light in vacuum, and λ_0 the corresponding wavelength).

We note that for $\varepsilon'' = 0$ our scenario reduces to the case already studied in Ref. [33], for which wave tunneling was observed at a Brewster angle θ_B corresponding to the polaritonic resonance of the slab

$$k_{x0} = k_0 \sin\theta_B = k_0\sqrt{\varepsilon'}, \tag{5}$$

with angular bandwidth narrowing down for decreasing values of ε' and/or increasing values of $k_0 d$. The reader is also referred to Refs. [51,52] for other examples of total transmission through *anisotropic*, lossless ENZ slabs. On the other hand, in ENZ slabs characterized by slight (e.g., partially compensated) losses, a pseudo-Brewster angle can be identified for which reflection is strongly reduced due to a nonresonant impedance-matching condition [45].

Our study following complements the above results by identifying a different wave-tunneling phenomenon that can occur in ENZ bilayers with *balanced* loss and gain.

B. Observables

Referring to the incident fields in Fig. 1, and labeling with the superscripts (R) and (T) the corresponding reflected and transmitted fields, respectively, we define as meaningful observables the reflection coefficients for incidence from the

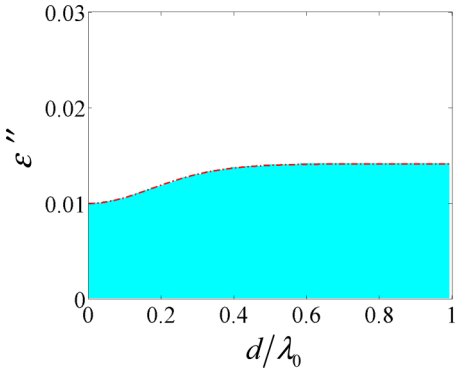

FIG. 2. (Color online) Configuration as in Fig. 1, but in the ENZ limit ($\varepsilon' = 10^{-4}$). The cyan-shaded area identifies parameter configurations (d/λ_0, ε'') for which a tunneling angle is numerically found. The dashed-dotted curve represents the approximate analytical bound in (22).

left and right

$$R_l \equiv \frac{H_l^{(R)}(x,-d)}{H_l^{(i)}(x,-d)}, \quad R_r \equiv \frac{H_r^{(R)}(x,d)}{H_r^{(i)}(x,d)}, \tag{6}$$

which are generally different, and a transmission coefficient

$$T \equiv \frac{H_l^{(T)}(x,d)}{H_l^{(i)}(x,-d)} = \frac{H_r^{(T)}(x,-d)}{H_r^{(i)}(x,d)}, \tag{7}$$

which is identical for both types of incidence, due to reciprocity. The above observables are related by a generalized unitarity relation [17]

$$R_l R_r = T^2\left(1 - \frac{1}{|T|^2}\right), \tag{8}$$

which, in turn, yields the conservation relation [17]

$$||T|^2 - 1| = |R_l R_r|. \tag{9}$$

III. MAIN ANALYTICAL AND NUMERICAL RESULTS

A. Reflection and transmission coefficients

The observables defined in (6) and (7) can be calculated analytically (see Appendix A for details). For the reflection coefficients, we obtain

$$R_{l,r}(\theta,k_0d,\varepsilon_1) \equiv \frac{N_1(\theta,k_0d,\varepsilon_1) \pm N_2(\theta,k_0d,\varepsilon_1)}{D(\theta,k_0d,\varepsilon_1)}, \tag{10}$$

where the + and − signs refer to the incidence from left (i.e., R_l) and right (i.e., R_r), respectively, and

$$N_1(\theta,k_0d,\varepsilon_1) = |k_{z1}|^2\mathrm{Re}(\varepsilon_1^* k_{z1}\tau_1) - |\varepsilon_1|^2 k_{z0}^2\mathrm{Re}(\varepsilon_1 k_{z1}^*\tau_1), \tag{11a}$$

$$\begin{aligned} N_2(\theta,k_0d,\varepsilon_1) &= k_{z0}|\tau_1|^2\mathrm{Re}\left[i\varepsilon_1^2(k_{z1}^*)^2\right] \\ &= \varepsilon'' k_0^3|\tau_1|^2\cos\theta \\ &\quad\times[(\varepsilon')^2 + (\varepsilon'')^2 - 2\varepsilon'\sin^2\theta], \end{aligned} \tag{11b}$$

$$\begin{aligned} D(\theta,k_0d,\varepsilon_1) &= ik_{z0}\left\{|\tau_1|^2\mathrm{Re}\left[\varepsilon_1^2(k_{z1}^*)^2\right] - |\varepsilon_1|^2|k_{z1}|^2\right\} \\ &\quad - |k_{z1}|^2\mathrm{Re}(\varepsilon_1 k_{z1}^*\tau_1^*) \\ &\quad - \mathrm{Re}\left(|\varepsilon_1|^2\varepsilon_1 k_{z0}^2 k_{z1}^*\tau_1\right), \end{aligned} \tag{12}$$

with

$$k_{z1} = k_0\sqrt{\varepsilon_1 - \sin^2\theta}, \quad \mathrm{Im}(k_{z1}) \leqslant 0, \tag{13}$$

$$\tau_1 = \tan(k_{z1}d). \tag{14}$$

The transmission coefficient can be instead written as

$$T(\theta,k_0d,\varepsilon_1) = \frac{-ik_{z0}|\varepsilon_1|^2|k_{z1}|^2\left|1+\tau_1^2\right|}{D(\theta,k_0d,\varepsilon_1)}. \tag{15}$$

B. Tunneling conditions

The tunneling (i.e., zero-reflection) conditions, for incidence from either side, can be derived from (10) by enforcing

$$N_1(\theta,k_0d,\varepsilon_1) \pm N_2(\theta,k_0d,\varepsilon_1) = 0, \tag{16}$$

subject to *a posteriori* verification that the denominator is nonzero. From (11b), it immediately follows that

$$N_2(\theta_c,k_0d,\varepsilon_1) = 0, \quad \theta_c = \arcsin\left[\sqrt{\frac{(\varepsilon')^2 + (\varepsilon'')^2}{2\varepsilon'}}\right]. \tag{17}$$

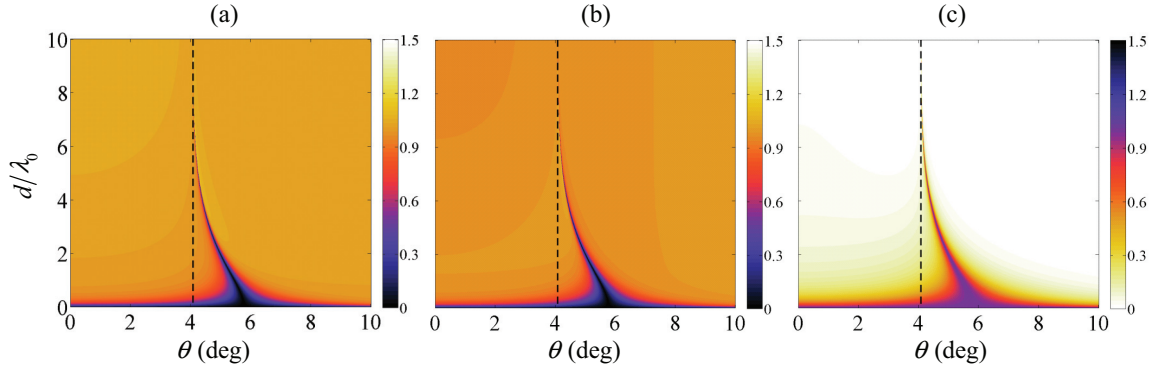

FIG. 3. (Color online) Observables (magnitude) in (10) and (15) as a function of θ and d/λ_0, for $\varepsilon' = 10^{-4}$, and $\varepsilon'' = 0.001$ ($\varepsilon'' < \varepsilon_l''$). (a) $|R_l|$, (b) $|R_r|$, (c) $|T|$. The vertical dashed lines indicate the critical angle $\theta_c = 4.07^\circ$ [cf. (17)].

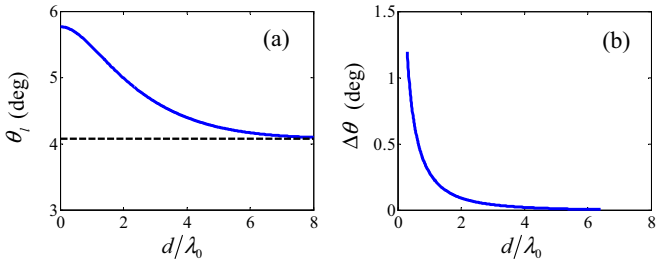

FIG. 4. (Color online) Parameters as in Fig. 3. (a) Tunneling angle (for incidence from left) θ_l as a function d/λ_0 [extracted from Fig. 3(a)]. (b) Corresponding full width at half maximum $\Delta\theta$ in the transmission response [numerically extracted from Fig. 3(c)]. The horizontal dashed line indicates the critical angle $\theta_c = 4.07^\circ$ [cf. (17)].

Moreover, it can be shown (see Appendix B for details) that

$$\lim_{k_0 d \to \infty} N_1\left(\theta_c, k_0 d, \varepsilon_1\right) = 0, \tag{18}$$

which implies that, for a sufficiently thick bilayer, the tunneling condition (in θ) approaches the critical angle θ_c in (17). Such angle, which admits real values for

$$\varepsilon'' \leqslant \varepsilon_u \equiv \sqrt{\varepsilon'\left(2-\varepsilon'\right)}, \tag{19}$$

is fundamentally different from the standard Brewster angle in a conventional (lossless, gainless) dielectric slab

$$\theta_B = \arctan\sqrt{\varepsilon'}, \tag{20}$$

and it is also not related to the polaritonic resonance of a lossless ENZ slab in (5) (see also the discussion in Sec. III C below). For a better understanding, we observe that the configuration in Fig. 1 may support (in the half-space limit $d \to \infty$) a surface wave exponentially bound along the z direction, characterized by the dispersion relationship [8,53]

$$k_x^{(SW)} = k_0\sqrt{\frac{\varepsilon_1\varepsilon_1^*}{\varepsilon_1+\varepsilon_1^*}} = k_0\sqrt{\frac{(\varepsilon')^2+(\varepsilon'')^2}{2\varepsilon'}}. \tag{21}$$

Interestingly, the inherent $\mathcal{PT}$ symmetry dictates that the propagation constant in (21) is *always real*. Moreover, it can be observed that the critical angle θ_c in (17) yields the phase-matching condition for the coupling of the impinging plane wave with the surface wave in (21).

C. Results

The above observations imply that, for moderate to large electrical thicknesses, the tunneling phenomenon is mediated by the excitation of a surface wave at the gain-loss interface $z = 0$. Nevertheless, the tunneling phenomenon can also be observed in electrically thin structures. In the ENZ limit, it can be shown (see Appendix C for details) that, for given bilayer permittivities and electrical thickness, there *always* exists an incidence angle yielding tunneling (from either side) within the interval $(\theta_c, \pi/2)$, provided that

$$\varepsilon'' \leqslant \sqrt{\frac{\varepsilon'\left(2-\varepsilon'\right)\left[\varepsilon' k_0 d\left(\tau_0^2-1\right)+2\tau_0\right]}{k_0 d\left(\varepsilon'-2\right)\left(\tau_0^2-1\right)+2\tau_0}},$$
$$\tau_0 = \tanh\left(k_0 d\right). \tag{22}$$

We note that real solutions of (22) exist if

$$\varepsilon' < \frac{2\tau_0}{k_0 d\left(1-\tau_0^2\right)}, \tag{23}$$

which is satisfied in the assumed ENZ limit. Moreover, we observe that, in the limit $k_0 d \to 0$ (i.e., $\tau_0 \to 0$), the bound in (22) reduces to

$$\varepsilon'' \leqslant \varepsilon_l'' \equiv \left(2-\varepsilon'\right)\sqrt{\frac{\varepsilon'}{4-\varepsilon'}}, \tag{24}$$

whereas, in the asymptotic limit $k_0 d \to \infty$ (i.e., $\tau_0 \to 1$), it reduces to the condition in (19), which ensures real values of the critical angle in (17).

For a representative small value of ε', Fig. 2 illustrates and numerically verifies the above bound via a bipartition of the relevant parameter space (ε'' versus d/λ_0) between a region (cyan shaded) where tunneling angles are numerically

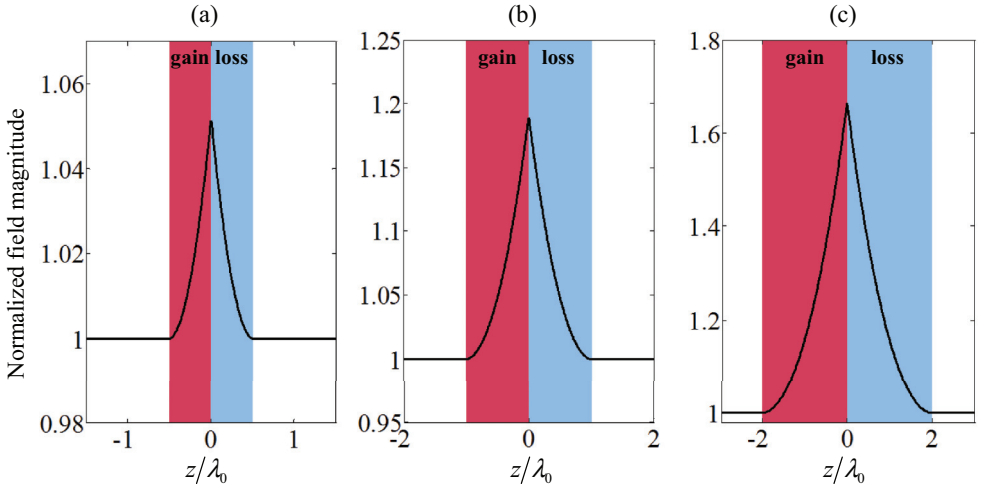

FIG. 5. (Color online) Parameters as in Fig. 3. Magnetic-field magnitude ($|H_y|$) distribution (normalized with respect to the incident field) along the z direction, for three representative values of d/λ_0, and corresponding tunneling angles [for incidence from left, cf. Fig. 4(a)]. (a) $d/\lambda_0 = 0.5$, $\theta = \theta_l = 5.66^\circ$, (b) $d/\lambda_0 = 1$, $\theta = \theta_l = 5.45^\circ$, (c) $d/\lambda_0 = 2$, $\theta = \theta_l = 4.97^\circ$. Note the different scales in the graphs.

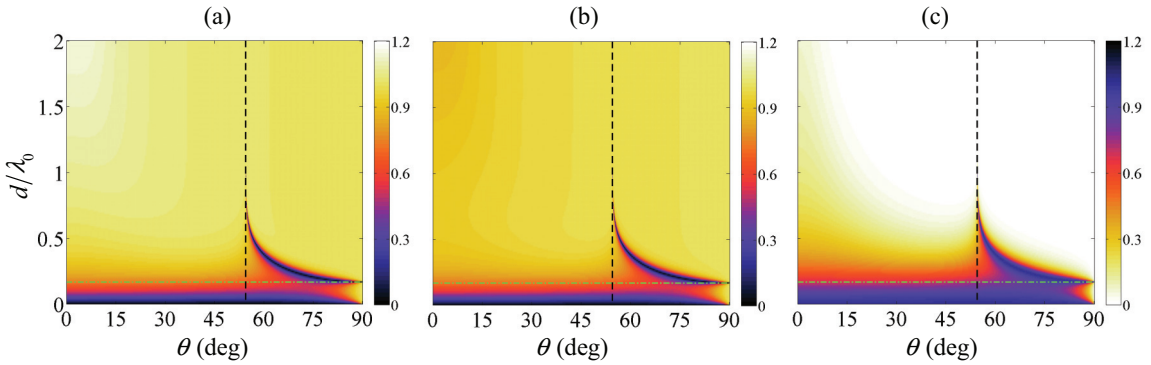

FIG. 6. (Color online) As in Fig. 3, but for $\varepsilon'' = 0.0115$. The horizontal dashed line indicates the critical value of d/λ_0 beyond which a tunneling angle should exist, according to the approximate estimate in (22).

found, and another region (white) where no solution can be found. As it can be observed, such numerical bipartition is in excellent agreement with the approximate estimate in (22). From Fig. 2, we can basically identify three representative parameter configurations, as detailed in the following.

1. $\varepsilon'' < \varepsilon_l''$

In this case, it is always possible to achieve tunneling with a real incidence angle $\theta_c < \theta < \pi/2$, for arbitrary values of the bilayer electrical thickness. This is illustrated in Fig. 3, which shows the reflection (from both sides) and transmission coefficient magnitudes, as a function of θ and d/λ_0. As predicted, it can be observed that, for any value of d/λ_0, and for either incidence sides, there always exists a tunneling angle. We note that, though quite similar, the responses for incidence from left ($|R_l|$) and right ($|R_r|$) are actually slightly different, so that a tunneling condition for incidence from left generally implies *nonzero reflection* for incidence from right; such *unidirectional* character will be discussed in more detail in Sec. IV. Moreover, we observe that, for increasing values of the electrical thickness, the reflection dips (and corresponding transmission peaks) gradually move from $\pi/2$ and asymptotically approach the critical angle θ_c in (17), becoming increasingly narrower. This is better quantified in Fig. 4, which shows the tunneling angle (for incidence from left) θ_l [numerically extracted from Fig. 3(a)] and corresponding full width at half maximum $\Delta\theta$ in the transmission response [numerically extracted from Fig. 3(c)] as a function of d/λ_0. The above results [together with (17)] allow, in principle, to engineer the phenomenon (in terms of tunneling direction and angular bandwidth) by acting on the bilayer electrical thickness and constitutive parameters.

For the same parameter configuration, Fig. 5 shows the magnetic-field distributions (along the z direction) corresponding to a tunneling condition for incidence from left, for three representative values of d/λ_0. The localized field distribution peaked at the interface $z = 0$ and field enhancement (increasing with increasing thickness values) confirm that the tunneling phenomenon is mediated by the excitation of a surface wave [cf. (21)].

We note that the parameter range of interest ($\varepsilon'' < \varepsilon_l''$) also includes the lossless (and gainless) limit $\varepsilon'' \to 0$, which was already studied in Ref. [33]. In this regime, recalling (11b), the tunneling condition in (16) becomes

$$N_1(\theta, k_0 d, \varepsilon_1) = 0, \tag{25}$$

which is obviously independent on the incidence side, and it can be shown to trivially reduce to the polaritonic resonance condition in (5).

2. $\varepsilon_l'' < \varepsilon'' < \varepsilon_u''$

In this case, from Fig. 2, we expect that tunneling angles exist only for values of d/λ_0 above a critical threshold. This is confirmed by the results in Figs. 6 and 7, which qualitatively differ from those in Figs. 3 and 4, respectively, only in the small-thickness region, wherein the reflection never vanishes. For larger values of d/λ_0, the behavior qualitatively resembles that observed in the previous example, with the reflection dips asymptotically approaching the critical angle θ_c in (17) and narrowing down. However, by comparison with the previous example, this asymptotic regime is approached for smaller values of the electrical thickness (note the different d/λ_0 scales). In this regime, the field distributions (not shown for brevity) qualitatively resemble those in Fig. 5.

3. $\varepsilon'' > \varepsilon_u''$

In this regime, tunneling conditions are no longer achievable. From the physical viewpoint, recalling (17) and (21), this is due to the impossibility of exciting a surface wave at the interface $z = 0$ with a propagating plane wave impinging from

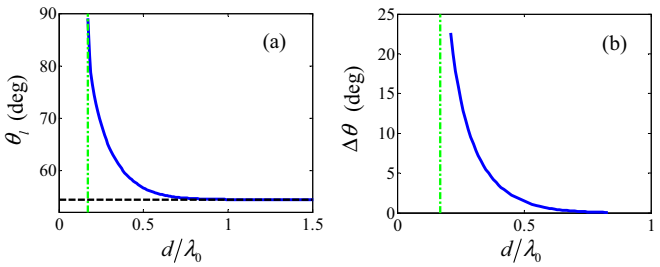

FIG. 7. (Color online) As in Fig. 4, but for $\varepsilon'' = 0.0115$. The horizontal dashed line indicates the critical angle $\theta_c = 54.41°$ [cf. (17)]. The vertical dashed-dotted line indicates the critical value $d/\lambda_0 = 0.17\lambda_0$ (cf. Fig. 2) beyond which a tunneling angle should exist, according to the approximate estimate in (22).

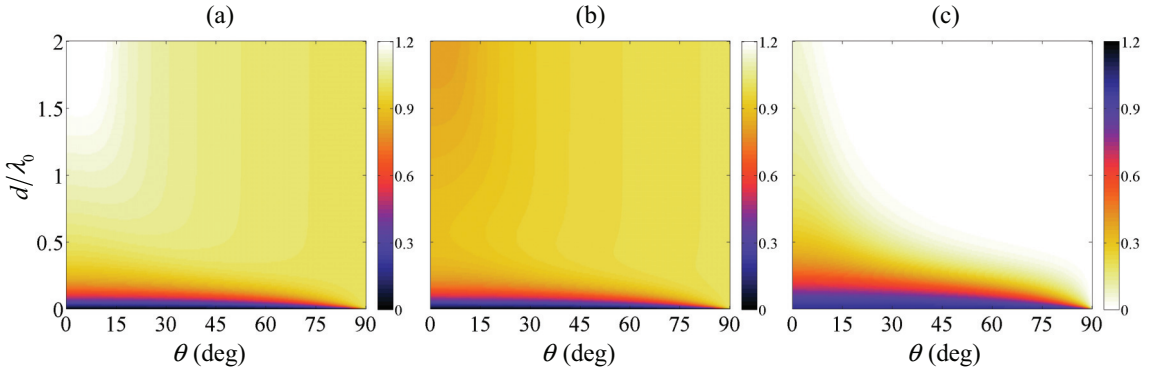

FIG. 8. (Color online) As in Fig. 3, but for $\varepsilon'' = 0.02$.

vacuum, i.e., with real values of the critical angle θ_c. This is illustrated in Fig. 8, which is markedly different from Figs. 3 and 6 above.

D. Remarks

We highlight that the possible excitation of a surface wave at the gain-loss interface $z = 0$, and hence the associated tunneling phenomenon, is not necessarily restricted to the insofar considered ENZ regime. From the mathematical viewpoint, the existence of a real-valued critical angle θ_c in (17) can be guaranteed by the condition $\varepsilon' < 2$ [cf. (19)]. However, it can be observed from (16) and (11b) that, for moderate values of ε' and $k_0 d$, this mechanism becomes effectively dominant only for values of ε'' corresponding to unfeasibly high levels of gain. This is exemplified in Fig. 9, which shows the reflection-coefficient magnitude for incidence from left (i.e., $|R_l|$), as a function of the incidence angle and electrical thickness, for a $\mathcal{PT}$-symmetric bilayer with $\varepsilon' = 1.5$ and three representative values of ε''. In particular, the reference case $\varepsilon'' = 0$ (i.e., no loss and gain) in Fig. 9(a) illustrates the standard Fabry-Perot–type oscillations, as well as the standard Brewster-angle condition typical of dielectric slabs for oblique, TM illumination. Very similar results can be observed for a configuration featuring low levels of loss and gain [$\varepsilon'' = 0.001$, cf. Fig. 9(b)]. By further increasing ε'' up to high levels of gain [$\varepsilon'' = 0.1$, cf. Fig. 9(c)], the tunneling phenomenon becomes barely visible, with the zero-reflection ridge disappearing at the standard Brewster angle $\theta_B = 56.3^\circ$ in (20), and gradually appearing (beyond a critical thickness value) at the critical angle $\theta_c = 60.22^\circ$ given by (17). In order to obtain a markedly visible phenomenon (as in Fig. 3), one would need unfeasibly high levels of gain. These observations motivate our focus on the ENZ regime, for which the tunneling phenomenon is attainable even in the presence of moderate-to-small electrical thicknesses and low levels of gain and loss.

IV. SPONTANEOUS SYMMETRY BREAKING

As previously mentioned, the symmetry condition $\varepsilon(z) = \varepsilon^*(-z)$ exhibited by the bilayer in Fig. 1 is only a necessary, but not sufficient, condition for the eigenspectrum to be real [3]. For given frequency and incidence direction, beyond a critical threshold of loss/gain level, the so-called "spontaneous symmetry breaking" may occur, i.e., an abrupt phase transition to a *complex* eigenspectrum [3].

In what follows, we investigate this phenomenon by utilizing a standard approach, already applied successfully to

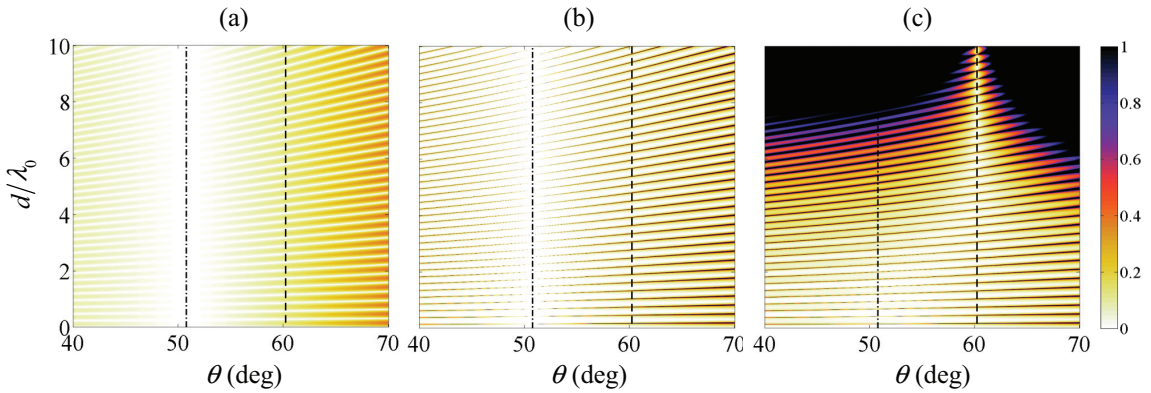

FIG. 9. (Color online) Reflection-coefficient magnitude (for incidence from left) $|R_l|$ as a function of the incidence angle θ and the bilayer electrical (semi)thickness d/λ_0, for $\varepsilon' = 1.5$ and three representative values of ε'': (a) $\varepsilon'' = 0$, (b) $\varepsilon'' = 0.001$, (c) $\varepsilon'' = 0.1$. The vertical dashed and dashed-dotted lines indicate the critical angle $\theta_c = 60.22^\circ$ [cf. (17)] and the Brewster angle $\theta_B = 50.77^\circ$ [cf. (20)] pertaining to a dielectric slab of relative permittivity ε', respectively.

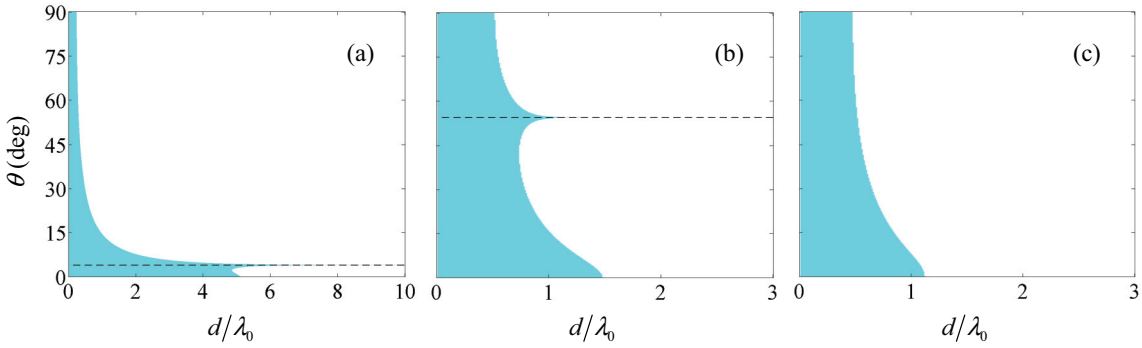

FIG. 10. (Color online) Illustration of the spontaneous symmetry-breaking phenomenon, for $\varepsilon' = 10^{-4}$, and representative values of ε''. The cyan-shaded regions indicate the parameters configurations $(d/\lambda_0, \theta)$ for which the eigenvalues of the scattering matrix $\underline{\underline{S}}_0$ in (26) are unimodular ($|\sigma_1| = |\sigma_2| = 1$), as a function of θ and d/λ_0: (a) $\varepsilon'' = 0.001$, (b) $\varepsilon'' = 0.0115$, (c) $\varepsilon'' = 0.02$. The horizontal dashed line indicates the critical angle θ_c [cf. (17)].

similar configurations [17], which studies the scattering matrix

$$\underline{\underline{S}}_0 = \begin{bmatrix} R_l & T \\ T & R_r \end{bmatrix}. \tag{26}$$

It can be shown that the eigenvalues σ_1 and σ_2 of such matrix are either both unimodular or of reciprocal magnitude [17], viz.,

$$|\sigma_1 \sigma_2| = 1, \tag{27}$$

with the two conditions $|\sigma_1| = |\sigma_2| = 1$ and $|\sigma_1| = 1/|\sigma_2| > 1$ characterizing the so-called "symmetric" and "broken" phases, respectively [17]. The transition (usually referred to as "exceptional point") between these two phases was shown to be closely related to the transition (from real to conjugate pairs) of the natural frequencies of the system in the complex frequency plane, i.e., the onset of spontaneous symmetry breaking [17]. Accordingly, we monitor such transitions as a function of the frequency and incidence direction for a given level of loss and gain, or, equivalently, as a function of the gain/loss level for given frequency and incidence angle.

Figure 10 illustrates this phenomenon, for three representative values of ε'' (corresponding to those chosen in Figs. 3, 6, and 8 above), by highlighting (cyan shading) the regions in the parameter space $(d/\lambda_0, \theta)$ where the eigenvalues σ_1 and σ_2 of the scattering matrix $\underline{\underline{S}}_0$ in (26) stay unimodular. It can be observed that, for a given value of ε'' and incidence angle, there exists a critical thickness value at which this transition occurs. For increasing values of ε'', this transition tends to occur at smaller values of θ and d/λ_0. It is also interesting to observe that, for incidence directions approaching the critical angle in (17), the transition tends to occur at increasingly higher values of d/λ_0 [cf. Figs. 10(a) and 10(b)]. This is better quantified in Fig. 11, which, for the case $\varepsilon'' = 0.001$, shows the magnitude of the two eigenvalues as a function of d/λ_0, for three incidence angles. It can be observed that, approaching the critical angle, the exceptional point moves towards increasingly larger values of d/λ_0. This is not surprising since we have shown analytically that, in the asymptotic limit $k_0 d \to \infty$ [also recalling (9)],

$$R_l \to 0, \quad R_r \to 0, \quad |T| \to 1, \tag{28}$$

which implies that the eigenvalues of scattering matrix in (26) are both unimodular. In these conditions, no symmetry breaking occurs.

As previously mentioned, the tunneling conditions are generally different for the incidence from left and right, and hence the phenomenon belongs to the general class of *anisotropic transmission resonances* [17,30]. These phenomena, which feature zero reflection occurring only for incidence from one side of the structure and not from the other, have been observed in several $\mathcal{PT}$-symmetric systems, and have been associated

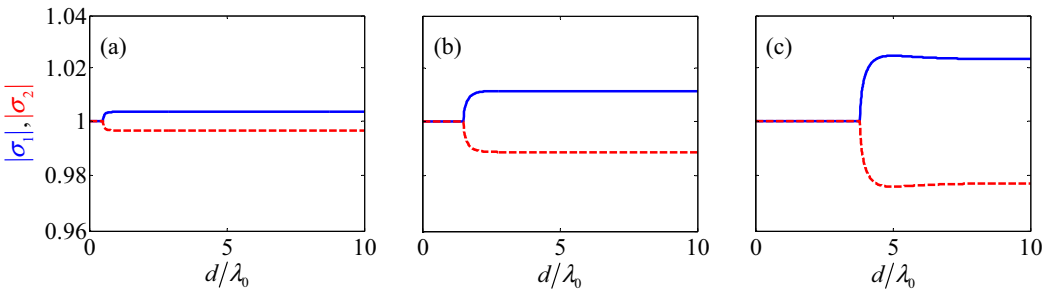

FIG. 11. (Color online) As in Fig. 10(a) ($\varepsilon'' = 0.001$), but magnitude (in semi-log scale) of eigenvalues σ_1 (blue solid line) and σ_2 (red dashed line) as a function of d/λ_0, for three representative incidence angles: (a) $\theta = 30^\circ$, (b) $\theta = 10^\circ$, (c) $\theta = 5^\circ$.

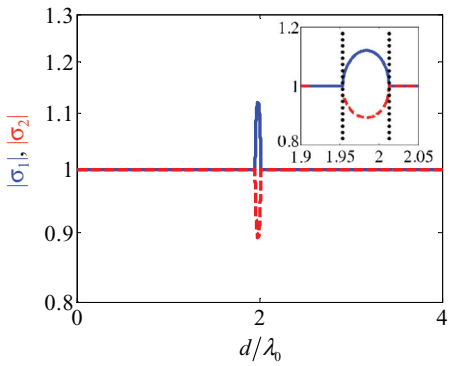

FIG. 12. (Color online) As in Fig. 11 ($\varepsilon'' = 0.001$), but eigenvalues of the scattering matrix $\underline{\underline{S}}_c$ in (29), for $\theta = 5^\circ$. The inset shows a magnified detail around the two exceptional points, which correspond to the tunneling conditions (vertical dotted lines) for incidence from the left ($R_l = 0$, at $d/\lambda_0 = 1.95$) and right ($R_r = 0$, at $d/\lambda_0 = 2.01$).

with exceptional points of the scattering matrix [14,17]

$$\underline{\underline{S}}_c = \begin{bmatrix} T & R_l \\ R_r & T \end{bmatrix}, \tag{29}$$

which differs from that in (26) by a mere permutation of its elements. The eigenvalues of this new scattering matrix $\underline{\underline{S}}_c$ (although different from those of $\underline{\underline{S}}_0$) exhibit the same property as in (27). Moreover, while the matrix $\underline{\underline{S}}_0$ above exhibits a *single* transition [17], the matrix $\underline{\underline{S}}_c$ may exhibit *multiple* exceptional points, which correspond to anisotropic transmission resonances. This is exemplified in Fig. 12, which, for the case $\varepsilon'' = 0.001$ and $\theta = 5^\circ$, shows the magnitude of the two eigenvalues as a function of d/λ_0. Two exceptional points can be observed, corresponding to the tunneling conditions for incidence from left and right (see also the magnified details in the inset).

V. CONCLUSIONS AND OUTLOOK

We have investigated tunneling phenomena that can occur in a $\mathcal{PT}$-symmetric ENZ bilayer under obliquely incident, TM-polarized plane-wave illumination. In particular, we have derived simple analytical conditions which parametrize the phenomenon, and also allow its physical interpretation in terms of the excitation of a surface wave localized at the gain-loss interface. We have also identified a critical threshold of the level of gain and loss, below which the tunneling phenomenon may occur. Beyond a critical electrical thickness, the incidence direction at which the phenomenon occurs approaches a critical angle dictated by the surface-wave phase-matching condition. Although the occurrence of this phenomenon is not strictly limited to the ENZ limit, in such a regime much lower levels of loss and gain, and only moderately thick (wavelength sized) structures are required.

Finally, via a spectral analysis, we have characterized the unidirectional character of this tunneling phenomenon, as well as the spontaneous symmetry breaking (i.e., transition from a real-valued to a complex-valued eigenspectrum) that can occur in this type of bilayers. The results from our prototype study constitute an interesting example of a tunneling phenomenon that is inherently induced by $\mathcal{PT}$ symmetry, and may provide new perspectives in the effect of low levels of balanced loss and gain in ENZ materials. Current and future investigations are aimed at the study of more realistic configurations (based, e.g., on metal-dielectric multilayers), taking also into account the arising spatial dispersion.

APPENDIX A: DETAILS ON THE DERIVATION OF EQS. (10) AND (15)

Assuming incidence from left, the y-directed magnetic field distribution in the various regions of Fig. 1 can be expressed as

$$H_y(x,z) = \exp(ik_{x0}x)\begin{cases} \exp[ik_{z0}(z+d)] + B_0\exp[-ik_{z0}(z+d)], & z < -d \\ A_1\exp(ik_{z1}z) + B_1\exp(-ik_{z1}z), & -d < z < 0 \\ A_2\exp(ik_{z1}^*z) + B_2\exp(-ik_{z1}^*z), & 0 < z < d \\ A_3\exp[ik_{z0}(z-d)], & z > d \end{cases} \tag{A1}$$

with k_{x0} and k_{z0} given in (4), k_{z1} given in (13), and the six unknown expansion coefficients $B_0, A_1, B_1, A_2, B_2, A_3$ to be calculated by enforcing the tangential-field continuity at the three interfaces $z = \pm d$ and 0. Within this framework, the tangential electric field can be derived from (A1) and the appropriate Maxwell's curl equation, viz.,

$$E_x(x,z) = \frac{\eta_0}{ik_0\varepsilon(z)}\frac{\partial H_y}{\partial z}(x,z), \tag{A2}$$

with η_0 denoting the vacuum characteristic impedance, and

$$\varepsilon(z) = \begin{cases} 1, & |z| > d \\ \varepsilon_1, & -d < z < 0 \\ \varepsilon_1^*, & 0 < z < d. \end{cases} \tag{A3}$$

In particular, we focus on the coefficients B_0 and A_3, which [cf. (6) and (7)] play the role of the reflection and transmission coefficients. After cumbersome yet straightforward analytical manipulations, we obtain

$$R_l = B_0 \equiv \frac{N_{Rl}}{D}, \tag{A4a}$$

$$N_{Rl} = \varepsilon_1 k_{z1}\tau_1^*[(\varepsilon_1^* k_{z0})^2 - (k_{z1}^*)^2] + \varepsilon_1^* k_{z1}^2\tau_1(i\varepsilon_1^* k_{z0}\tau_1^* - k_{z1}^*) + \varepsilon_1^2 k_{z0}k_{z1}^*\tau_1(\varepsilon_1^* k_{z0} + ik_{z1}^*\tau_1^*), \tag{A4b}$$

$$D = \varepsilon_1^* k_{z1}^2\tau_1(k_{z1}^* - i\varepsilon_1^* k_{z0}\tau_1^*) + \varepsilon_1^2 k_{z0}k_{z1}^*\tau_1(\varepsilon_1^* k_{z0} - ik_{z1}^*\tau_1^*) + \varepsilon_1 k_{z1}\left[2i\varepsilon_1^* k_{z0}k_{z1}^* + (\varepsilon_1^*)^2 k_{z0}^2\tau_1^* + (k_{z1}^*)^2\tau_1^*\right], \tag{A4c}$$

$$T = A_3 = \frac{2ik_{z0}|\varepsilon_1|^2|k_{z1}|^2\sec(k_{z1}d)\sec(k_{z1}^*d)}{D}. \tag{A5}$$

The final results in (10) and (15) follow from further simplifications which exploit the $\mathcal{PT}$-symmetric character.

The reflection coefficient for incidence from right (R_r) can be computed by repeating the above analysis with the proper excitation or, more directly, by substituting ε_1 and k_{z1} with their complex conjugates (and vice versa) in (10).

APPENDIX B: DETAILS ON EQ. (18)

First, we note from (13) and (17) that

$$k_{z1}|_{\theta=\theta_c} = \frac{\varepsilon_1 k_0}{\sqrt{2\varepsilon'}}. \tag{B1}$$

Moreover, it readily follows from (14) that

$$\lim_{k_0 d\to\infty} \tau_1 = -i. \tag{B2}$$

By substituting (B1) and (B2) in (11a), we obtain

$$\lim_{k_0 d\to\infty} N_1(\theta_c, k_0 d, \varepsilon_1) = |\varepsilon_1|^2 k_0 \left[\frac{k_{z0}^2}{\sqrt{2\varepsilon'}} - \frac{k_0^2}{(2\varepsilon')^{\frac{3}{2}}}\right] \times \mathrm{Re}(i\,|\varepsilon_1|^2) = 0, \tag{B3}$$

which corresponds to (18).

APPENDIX C: DETAILS ON EQ. (22)

In the ENZ limit (2), we can neglect the term proportional to $|\varepsilon_1|^2$ in (11a), so that

$$N_1(\theta, k_0 d, \varepsilon_1) \approx |k_{z1}|^2 \mathrm{Re}(\varepsilon_1^* k_{z1} \tau_1). \tag{C1}$$

In what follows, we determine the conditions under which a solution in θ of (16) [with (C1)] can be bracketed within the interval $(\theta_c, \pi/2)$.

First, we note from (11b) and (17) that the term N_2 vanishes for both $\theta = \theta_c$ and $\pi/2$. Moreover, from (14) and (B1), we obtain

$$\tau_1|_{\theta=\theta_c} = \tan\left(\frac{\varepsilon_1 k_0 d}{\sqrt{2\varepsilon'}}\right), \tag{C2}$$

which, substituted in (C1) [with (B1)], yields

$$N_1(\theta_c, k_0 d, \varepsilon_1) \approx \frac{|\varepsilon_1|^4 k_0^3}{(2\varepsilon')^{\frac{3}{2}}} \mathrm{Re}\left[\tan\left(\frac{\varepsilon_1 k_0 d}{\sqrt{2\varepsilon'}}\right)\right]. \tag{C3}$$

Recalling the behavior of the complex-argument tangent [54], we observe that the term N_1 is positive for

$$\mathrm{Re}\left(\frac{\varepsilon_1 k_0 d}{\sqrt{2\varepsilon'}}\right) \lesssim \frac{\pi}{2}, \tag{C4}$$

which implies that

$$\frac{d}{\lambda_0} \lesssim \frac{1}{4}\sqrt{\frac{2}{\varepsilon'}}. \tag{C5}$$

We note that, in the ENZ limit $\varepsilon' \ll 1$, the condition in (C5) is verified for electrical thicknesses up to moderately large values. For instance, assuming $\varepsilon' = 10^{-4}$, the condition is satisfied for $d/\lambda_0 \lesssim 35$, i.e., well within the parameter range of interest. Therefore, we can conclude that the left-hand side in (C1) is positive at $\theta = \theta_c$.

Next, we observe from (13) that

$$k_{z1}|_{\theta=\frac{\pi}{2}} = k_0\sqrt{\varepsilon_1 - 1} \approx k_0\left(\frac{\varepsilon_1}{2} - i\right), \tag{C6}$$

where the approximate equality stems from a first-order McLaurin expansion (in ε_1). Similarly, by first-order McLaurin expansion (in ε_1) of τ_1 in (14), we obtain

$$\tau_1|_{\theta=\frac{\pi}{2}} \approx -i\tau_0 - i\frac{\varepsilon_1 k_0 d}{2}\left(\tau_0^2 - 1\right), \tag{C7}$$

with τ_0 defined in (22). By substituting (C6) and (C7) in (C1), we obtain

$$N_1\left(\frac{\pi}{2}, k_0 d, \varepsilon_1\right) \approx \frac{k_0^3\,|\varepsilon_1 - 1|}{4}\left[2\tau_0(|\varepsilon_1|^2 - 2\varepsilon') + |\varepsilon_1|^2 k_0 d(\varepsilon' - 2)\left(\tau_0^2 - 1\right)\right]. \tag{C8}$$

The condition in (22) follows by enforcing that the expression in (C8) is negative, so that a solution of (C1) can be bracketed within the interval $(\theta_c, \pi/2)$. We verified numerically that, within the parameter range of interest, N_1 is a monotonic function of θ, and hence the above condition is not only sufficient, but also necessary. We stress that this result does not depend on the incidence side.

[1] C. M. Bender and S. Boettcher, Phys. Rev. Lett. **80**, 5243 (1998).
[2] C. M. Bender, S. Boettcher, and P. N. Meisinger, J. Math. Phys. **40**, 2201 (1999).
[3] C. M. Bender, Rep. Prog. Phys. **70**, 947 (2007).
[4] M. K. Oberthaler, R. Abfalterer, S. Bernet, J. Schmiedmayer, and A. Zeilinger, Phys. Rev. Lett. **77**, 4980 (1996).
[5] A. Guo, G. J. Salamo, D. Duchesne, R. Morandotti, M. Volatier-Ravat, V. Aimez, G. A. Siviloglou, and D. N. Christodoulides, Phys. Rev. Lett. **103**, 093902 (2009).
[6] C. E. Rüter, K. G. Makris, R. El-Ganainy, D. N. Christodoulides, M. Segev, and D. Kip, Nat. Phys. **6**, 192 (2010).
[7] A. Mostafazadeh, Phys. Rev. Lett. **102**, 220402 (2009).
[8] J. Čtyroký, V. Kuzmiak, and S. Eyderman, Opt. Express **18**, 21585 (2010).
[9] A. Mostafazadeh and M. Sarsaman, Phys. Lett. A **375**, 3387 (2011).
[10] H. F. Jones, J. Phys. A: Math. Theor. **44**, 345302 (2011).
[11] H. Benisty, A. Degiron, A. Lupu, A. De Lustrac, S. Chénais, S. Forget, M. Besbes, G. Barbillon, A. Bruyant, S. Blaize, and G. Lérondel, Opt. Express **19**, 18004 (2011).
[12] A. E. Miroshnichenko, B. A. Malomed, and Y. S. Kivshar, Phys. Rev. A **84**, 012123 (2011).
[13] Y. D. Chong, L. Ge, and A. D. Stone, Phys. Rev. Lett. **106**, 093902 (2011).
[14] S. Longhi, J. Phys. A: Math. Theor. **44**, 485302 (2011).
[15] H. F. Jones, J. Phys. A: Math. Theor. **45**, 135306 (2012).
[16] M.-A. Miri, P. LiKamWa, and D. N. Christodoulides, Opt. Lett. **37**, 764 (2012).

[17] L. Ge, Y. D. Chong, and A. D. Stone, Phys. Rev. A **85**, 023802 (2012).
[18] S. Yu, X. Piao, D. R. Mason, S. In, and N. Park, Phys. Rev. A **86**, 031802(R) (2012).
[19] H. Alaeian and J. A. Dionne, arXiv:1306.0059.
[20] M. Kang, F. Liu, and J. Li, Phys. Rev. A **87**, 053824 (2013).
[21] G. Castaldi, S. Savoia, V. Galdi, A. Alù, and N. Engheta, Phys. Rev. Lett. **110**, 173901 (2013).
[22] M.-A. Miri, M. Heinrich, and D. N. Christodoulides, Phys. Rev. A **87**, 043819 (2013).
[23] M. Kulishov, B. Kress, and R. Slavík, Opt. Express **21**, 9473 (2013).
[24] X. Luo, J. Huang, H. Zhong, X. Qin, Q. Xie, Y. S. Kivshar, and C. Lee, Phys. Rev. Lett. **110**, 243902 (2013).
[25] A. Regensburger, C. Bersch, M.-A. Miri, G. Onishchukov, D. N. Christodoulides, and U. Peschel, Nature (London) **488**, 167 (2012).
[26] L. Feng, Y.-L. Xu, W. S. Fegadolli, M.-H. Lu, J. E. B. Oliveira, V. R. Almeida, Y.-F. Chen, and A. Scherer, Nat. Mater. **12**, 108 (2012).
[27] A. Regensburger, M.-A. Miri, C. Bersch, J. Näger, G. Onishchukov, D. N. Christodoulides, and U. Peschel, Phys. Rev. Lett. **110**, 223902 (2013).
[28] S. Longhi and G. Della Valle, Phys. Rev. A **85**, 012112 (2012).
[29] J. Schindler, Z. Lin, J. M. Lee, H. Ramezani, F. M. Ellis, and T. Kottos, J. Phys. A: Math. Theor. **45**, 444029 (2012).
[30] Z. Lin, J. Schindler, F. M. Ellis, and T. Kottos, Phys. Rev. A **85**, 050101 (2012).
[31] N. Engheta, Science **340**, 286 (2013).
[32] M. G. Silveirinha and N. Engheta, Phys. Rev. Lett. **97**, 157403 (2006).
[33] A. Alù, M. G. Silveirinha, A. Salandrino, and N. Engheta, Phys. Rev. B **75**, 155410 (2007).
[34] A. Alù and N. Engheta, Phys. Rev. B **78**, 045102 (2008).
[35] A. Alù and N. Engheta, Phys. Rev. Lett. **103**, 043902 (2009).
[36] Ernst Jan R. Vesseur, T. Coenen, H. Caglayan, N. Engheta, and A. Polman, Phys. Rev. Lett. **110**, 013902 (2013).
[37] C. Rizza, A. Ciattoni, and E. Palange, Phys. Rev. A **83**, 053805 (2011).
[38] C. Argyropoulos, P.-Y. Chen, G. D'Aguanno, N. Engheta, and A. Alù, Phys. Rev. B **85**, 045129 (2012).
[39] M. A. Vincenti, D. de Ceglia, A. Ciattoni, and M. Scalora, Phys. Rev. A **84**, 063826 (2011).
[40] G. Castaldi, S. Savoia, V. Galdi, A. Alù, and N. Engheta, Phys. Rev. B **86**, 115123 (2012).
[41] G. Castaldi, V. Galdi, A. Alù, and N. Engheta, Phys. Rev. Lett. **108**, 063902 (2012).
[42] S. Campione, D. de Ceglia, M. A. Vincenti, M. Scalora, and F. Capolino, Phys. Rev. B **87**, 035120 (2013).
[43] C. Rizza, A. Di Falco, and A. Ciattoni, Appl. Phys. Lett. **99**, 221107 (2011).
[44] S. Campione, M. Albani, and F. Capolino, Opt. Mater. Express **1**, 1077 (2011).
[45] D. de Ceglia, S. Campione, M. A. Vincenti, F. Capolino, and M. Scalora, Phys. Rev. B **87**, 155140 (2013).
[46] Y. Jin, S. Xiao, N. A. Mortensen, and S. He, Opt. Express **19**, 11114 (2011).
[47] L. Sun, S. Feng, and X. Yang, Appl. Phys. Lett. **101**, 241101 (2012).
[48] S. Feng and K. Halterman, Phys. Rev. B **86**, 165103 (2012).
[49] S. Feng, Phys. Rev. Lett. **108**, 193904 (2012).
[50] M. A. Vincenti, S. Campione, D. de Ceglia, F. Capolino, and M. Scalora, New J. Phys. **14**, 103016 (2012).
[51] L.-Z. Lu, J.-J. Wang, and Y.-T. Fang, Opt. Laser Technol. **47**, 4 (2013).
[52] J. Luo, Y. Xu, H. Chen, B. Hou, W. Lu, and Y. Lai, Europhys. Lett. **101**, 44001 (2013).
[53] M. Nezhad, K. Tetz, and Y. Fainman, Opt. Express **12**, 4072 (2004).
[54] M. Abramowitz and I. Stegun, *Handbook of Mathematical Functions* (Dover, New York, 1964).